Official Journal of CIOMP
elight.springeropen.com

REVIEW

Open Access

Optical spatiotemporal vortices

Chenhao Wan[1,2], Andy Chong[3] and Qiwen Zhan[1,4,5*]

Abstract

Spatiotemporal vortices of light, featuring transverse orbital angular momentum (OAM) and energy circulation in the spatiotemporal domain, have received increasing attention recently. The experimental realization of the controllable generation of spatiotemporal vortices triggers a series of research in this field. This review article covers the latest developments of spatiotemporal vortices of light ranging from theoretical physics, experimental generation schemes, and characterization methods, to applications and future perspectives. This new degree of freedom in photonic OAM endowed by spatiotemporal vortices paves the way to the discovery of novel physical mechanisms and photonic applications in light science.

Keywords Spatiotemporal optical vortex, Orbital angular momentum, Spin–orbit interaction, Linear momentum density, Toroidal vortex, Topological charge

1 Main text

Vortices of light, null regions of intensity surrounded by spiral phases, constitute the skeleton of a wavefield and influence the properties of light. Since the discovery of the tight connection of optical vortices and orbital angular momentum (OAM) of light in the seminal paper in 1992 [1], considerable research progress has been made to unveil the beauty of vortices of light. Numerous applications of optical OAM have been discovered in both classic and quantum optics [2], including optical communication [3], quantum entanglement and cryptography [4–6], optical tweezing [7], driving torque for a micromachine [8], rotational Doppler shift [9], and imaging [10–12]. Optical vortices feature azimuthal phase dependence of $\exp(il\phi)$ where l is an integer known as the topological charge. The OAM carried by each photon is proportional to the topological charge and quantized in units of ħ. The spin angular momentum (SAM), associated with circular polarization states, is limited to [−ħ, ħ] per photon. The OAM per photon, however, is theoretically unbounded. The direction of angular momentum of light is usually directed along the propagation direction. A decade ago, the interest in transverse SAM started to emerge and transversely spinning electric fields were discovered in strongly focused beams and evanescent waves [13–24]. The word "photonic wheel" is coined to describe the orthogonal relationship of the SAM direction and the propagation direction. Analogously, optical vortices carrying transverse OAM have attracted rapidly growing interest [25]. Tilted vortices of light were predicted using the special theory of relativity [26]. A spatial optical vortex is seen by a transversely moving observer near the speed of light as a tilted vortex. Spatiotemporal optical vortices (STOVs), occupying a small fraction of total energy, were observed in femtosecond filaments in air [27]. Controllable generation of STOVs with transverse OAM were demonstrated in a linear manner [28, 29]. Second harmonic generation (SHG) of transverse OAM were reported and the conservation of OAM was demonstrated [30, 31]. Rigorous calculation of transverse OAM

*Correspondence:
Qiwen Zhan
qwzhan@usst.edu.cn
[1] School of Optical-Electrical and Computer Engineering, University of Shanghai for Science and Technology, Shanghai 200093, China
[2] School of Optical and Electronic Information and Wuhan National Laboratory for Optoelectronics, Huazhong University of Science and Technology, Wuhan 430074, Hubei, China
[3] Department of Physics, Pusan National University, Geumjeong-Gu, Busan 46241, South Korea
[4] Zhangjiang Laboratory, 100 Haike Road, Shanghai 201204, China
[5] Shanghai Key Lab of Modern Optical System, University of Shanghai for Science and Technology, Shanghai 200093, China

and the coupling of transverse OAM and SAM were accomplished [32–34]. Schemes were designed to generate STOVs using metasurfaces and photonic crystals [35–37]. Undoubtedly, the experimental realization of STOVs has been driving the increasing interest in STOVs and spurring their potential applications in various optical phenomena. This review article is intended to cover the latest research progress in the field of spatiotemporal vortices in optics. The mathematical theory and physical interpretation are presented in Sect. 2. The generation, propagation and conversion of STOVs are discussed in Sect. 3. Section 4 reviews the current characterization methods and their limitations. Section 5 introduces different types of STOVs. The applications of STOVs are discussed in Sect. 6. Future perspectives on STOVs are concluded in the summary. It should be noted that this article focuses on the very recent advances related to STOVs. Readers interested in the latest developments of more general spatiotemporal wave packets and structured waves may refer to review articles [38, 39].

2 Mathematical expression and physical interpretation

2.1 Mathematical expression

The mathematical expression of an optical wave field is generally a function of the three-dimensional (3D) space and the one-dimensional (1D) time. The spatial and temporal dimensions are generally considered separable for simplification. In fact, the coupling of space and time is ubiquitous and becomes nonnegligible in cases of high intensity and tight focusing [40]. Spatiotemporal coupling is generally considered detrimental and regarded as side effects that should be avoided. Recently, interest has growing on exploiting the spatiotemporal coupling effect on purpose. Spatiotemporal light sheet is a typical example of spatiotemporal light field that has shown exotic features such as invariant propagation, controllable group velocity, and veiled Talbot effect [41–43].

The STOV is another quintessential example that takes advantage of the spatiotemporal coupling effect. In physics, the STOV belongs to a category of optical field that carries a spatiotemporal spiral phase. In contrast to conventional optical vortex that has a spiral phase expressed with two spatial dimensions, the STOV carries a spatiotemporal spiral phase expressed with one spatial coordinate and one temporal coordinate:

$$E(x,y,t,z) = A(x,y,z,t)\exp(il\varphi_{st})\exp[ik(z-vt)]. \tag{1}$$

Equation 1 expresses a STOV wave packet propagating in the z direction under paraxial and narrow band approximation, where $A(x,y,z,t)\exp(il\varphi_{st})$ is the complex envelope function, $l\varphi_{st}$ denotes the spatiotemporal spiral phase, k is the wave number of the central frequency. The azimuthal angle in the spatiotemporal plane, e.g. the x–t plane, can be expressed as

$$\varphi_{st} = \tan^{-1}\left(\frac{x/x_s}{\tau/\tau_s}\right), \tag{2}$$

where $\tau = z/v - t$ is the local time coordinate, x_s and τ_s are the widths of the wave packet along the x and τ directions. The normalization in Eq. (2) is necessary because the spatial coordinate and the temporal coordinate are in different units. The mathematical expression of a STOV shows that the spatial and temporal dimensions are coupled and nonseparable. The spatiotemporal coupling in the form of a vortex in the spatiotemporal domain is the most salient feature of a STOV where a number of novel physical phenomena originate from. It is worthy of noting that ultrashort pulses with other nontrivial spatiotemporal coupling and energy circulation in the transverse spatial dimensions are not classified as STOVs [44–50].

2.2 Physical interpretation: momentum density, angular momentum density, and transverse OAM

It is well known that light carries linear momentum. The momentum density (or optical current) can be decomposed into a dominant longitudinal component that represents the light propagation in the main direction, and a local component determined by the 3D phase structure of the wave packet given by [51],

$$\boldsymbol{J} = \mathrm{Im}\psi^*\nabla\psi, \tag{3}$$

where ψ is the envelope function, Im stands for imaginary part, * denotes complex conjugate, and ∇ is the nabla operator. The OAM density equals the cross product of the position vector $\boldsymbol{r}$ and the momentum density $\boldsymbol{J}$,

$$\boldsymbol{L} = \boldsymbol{r}\times\boldsymbol{J}. \tag{4}$$

The OAM per wave packet equals the volume integral of the OAM density $\boldsymbol{L}$. The average OAM per photon is the total OAM of the wave packet divided by the total number of photons contained in the wave packet. It is worthy of noting that the OAM is tightly connected to the spiral phase structure. A spiral phase structure, no matter in the spatial domain or the spatiotemporal domain, leads to space-dependent and tilted wave vectors. These tilted wave vectors, excluding the dominant longitudinal component, form circulating momentum density. For a spatial vortex, the momentum density circulates in the x–y plane, leading to an OAM density parallel to the z axis; For a STOV, the momentum density circulates in a spatiotemporal plane, e.g. x–t plane, resulting in an OAM density orthogonal to the z axis. The Poynting vector is

given by c^2 times the momentum density. The circulation of momentum density in a STOV indicates that a small fraction of energy circulates in the spatiotemporal domain while advancing at the speed of light along the propagation direction. This behavior of light resembles the movement of a cyclone where the rotating axis and the advancing direction are perpendicular to each other. The OAM carried by STOVs is named transverse OAM to differ from the longitudinal OAM carried by a spatial vortex beam. It is worthy of noting that there is lateral shift between the energy-density and photon (probability) centroid of a STOV. Choosing the probability centroid as the origin is preferred as discussed in [52].

3 Generation, propagation and conversion of STOVs

One theoretical paper was published in 2012 discussing how to observe a spatial vortex as a STOV [26]. However, the special theory of relativity and the requirement of a fast-moving observer makes it extremely difficult to realize a STOV in a laboratory. The STOV phenomenon was observed in the nonlinear collapse and self-arrest of an extremely intense optical pulse in air [27]. Only a small fraction of energy contributes to the phenomenon and there is no way to readily control the properties. The first controllable generation of STOVs was achieved only recently [28, 29, 53]. It circumvents the necessity of a fast-moving observer and requires neither complex nonlinear configuration nor high pulse energy.

The idea originates from the conservation of OAM of light in the spatiotemporal domain and in the spatiotemporal frequency domain. The creation of a spiral phase in the spatiotemporal domain is controlled by manipulating the phase structure in the spatiotemporal frequency domain. This breakthrough leads to the experimental generation of STOVs in a linear and manageable manner. The exploration of novel physical properties and potential applications of STOVs has since then become experimentally plausible.

Higher order STOVs are immediately observed to be easily breakable upon propagation into multiple unitary STOVs [28, 29, 54]. This linear phenomenon attributes to the imbalance between dispersion and diffraction that affect the broadening in the temporal and spatial dimensions. Detection schemes of STOVs are developed based on their diffraction properties in free space [55]. Nonlinear conversion such as second harmonic generation (SHG) and high harmonic generation (HHG) are studied and the conservation of OAM is verified.

3.1 Spiral phase modulation using 2D pulse shaper

A 2D pulse shaper consists of two diffraction gratings, two cylindrical lenses and a 2D bespoke phase element as shown in Fig. 1a. The phase element can be a spiral phase plate or a spatial light modulator (SLM) that implements a spiral phase modulation. The optical setup is positioned in a 4*f* configuration that the phase element, the cylindrical lenses and the gratings separated by one focal length. The diffraction grating disperses different wavelengths along the horizontal direction. The vertical direction in the SLM plane is considered as the spatial frequency direction. The SLM applies different phase to different wavelengths as well as to different spatial positions to introduce controllable spatiotemporal phase coupling. For the generation of STOVs, the SLM imprints a spiral phase in the spatiotemporal frequency plane. The spiral phase can have arbitrary topological charge with either positive or negative signs. The aspect ratio of the spiral phase pattern and the phase singularity position are tuned to obtain an optimized experimental result. The spiral phase applied by the SLM in the spatiotemporal frequency domain is maintained in the spatiotemporal domain through a 2D spatiotemporal Fourier transform.

3.2 Generation of STOV with nanostructures

Nanostructures of subwavelength feature size are versatile in controlling the amplitude, phase, and polarization of a light beam by choosing the material type, shape, and formation of subwavelength structures. The space-dependent and wavelength-dependent response makes nanostructures suitable for applying spatiotemporal modulation to a wave packet. Nanophotonic platforms have been successfully demonstrated for spatial OAM multiplexing, chiral engineering in isotropic materials, creating vortices in real space, momentum space, and the spatiotemporal domain [56–59]. Compared with the 2D pulse shaper, nanostructures are considerably compact and easily integratable. A spatiotemporal differentiator that breaks spatial mirror symmetry is designed and demonstrated to generate STOVs carrying transverse OAM without spatial or temporal Fourier transform [35]. As shown in Fig. 1b, the nanostructure is 1D periodic silicon structure with two rods per period of different heights and widths. The period of the structure is smaller than the wavelength, therefore, only the zeroth order light will be transmitted.

The parameters of the nanostructure are optimized to obtain a desired transmission spectrum function that is valid around $k_x = 0$ and $\Omega = 0$ and is given by,

$$H(k_x, \Omega) = C_x k_x + C_t \Omega, \tag{5}$$

where $\Omega = \omega - \omega_0$ is the angular frequency, C_x and C_t are two complex numbers that has a phase difference. The phase singularity in the spatiotemporal spectrum plane results in a spiral phase in the spatiotemporal plane. The

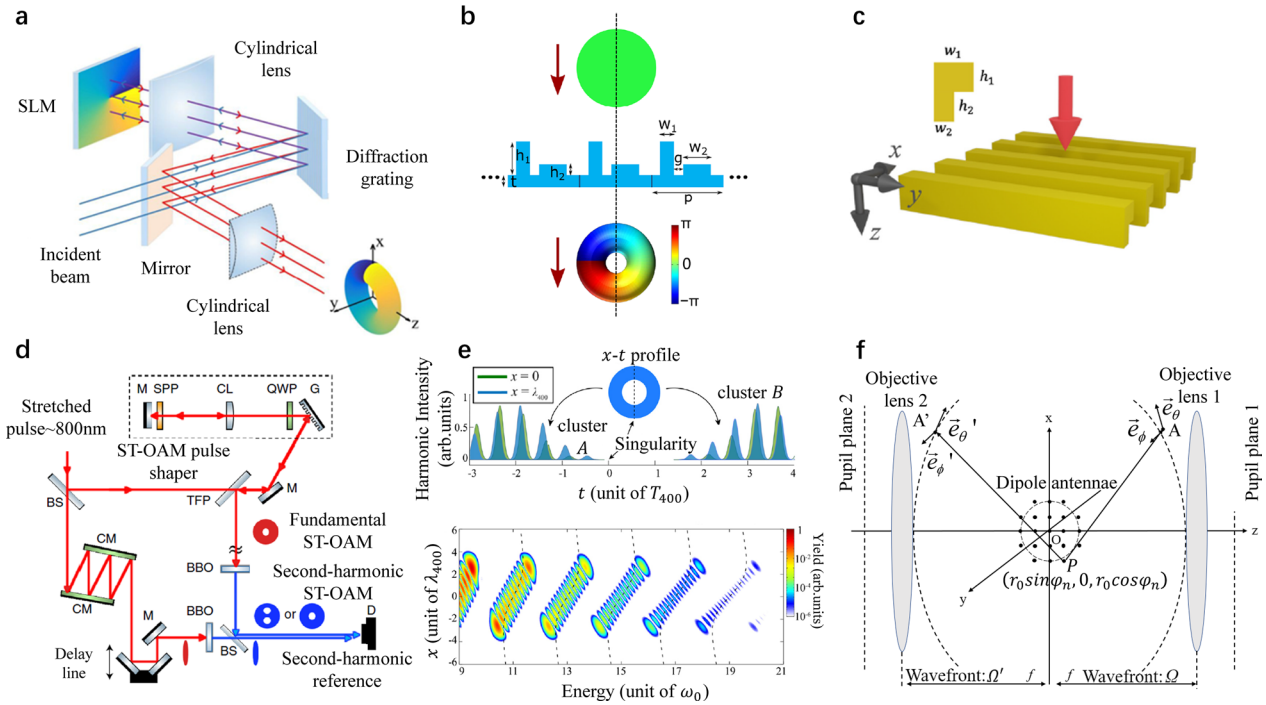

Fig. 1 Generation, propagation and conversion of STOVs. **a** Generation of STOVs through spiral phase modulation using 2D pulse shaper. Adapted with permission from [29], copyright 2020, NPG. **b** A spatiotemporal differentiator that breaks spatial mirror symmetry is capable of generating STOVs without Fourier transform. Adapted with permission from [35], copyright 2022, WILEY. **c** A photonic crystal slab structure that possesses a custom nodal line for the generation of STOVs. Adapted with permission from [37], copyright 2021, OPG. **d** STOVs under second harmonic nonlinear process. Adapted with permission from [31], copyright 2021, NPG. **e** High harmonic generation with transverse OAM. Adapted with permission from [63], copyright 2021, APS. **f** Focusing structured light to obtain focal field with transverse SAM and OAM. Adapted with permission from [65], copyright 2022, OPG

presented nanostructures are expected to be fabricated through standard lithography and etching processing [60, 61].

The topological property of nonlocal spatial-mirror-symmetry-breaking metasurfaces has also been investigated, adding a topological perspective for STOV generation using nanostructures [62]. All parameters in Fig. 1b are fixed except for the rod height h_1. For $h_1 < 230$ nm, no phase singularity is observed in the transmission spectrum function. For h_1 between 238.5 nm and 388.7 nm, the mirror symmetry is broken and phase singularities appear in the transmission map in pairs. For $h_1 > 388.7$ nm, h_1 is significantly taller than h_2 (160 nm), the phase singularity disappears. The transition from trivial case to topologically protected STOV and back to trivial case indicates the region where the STOV pulse can be generated and immune to fabrication imperfections. Randomly generated defects such as partial convexities, concavities, and various kinds of chamfers are introduced to verify the robustness of the structure for STOV generation. The topological robustness for STOV generation is crucial for the fabrication and integration of such nanostructures with other optoelectronic devices.

Another example is the design of a photonic crystal slab structure as shown in Fig. 1c that possesses a corresponding nodal line in its transmission spectrum function [37]. The transmission spectrum function is given by,

$$H(k_x, k_y, \Omega) = C_x k_x + C_y k_y \sin\beta - C_y \frac{\Omega}{c} \cos\beta, \quad (6)$$

where C_y is real, C_x is complex, and b characterizes the direction of the nodal line in the spatiotemporal frequency domain. An incident Gaussian pulse travels through the device and transforms into a STOV with its nodal line and OAM in arbitrary 3D direction.

3.3 Second harmonic generation (SHG)

The behavior of STOV pulses during frequency upconversion of SHG has been investigated [30, 31]. Using an experimental setup as shown in Fig. 1d, a fundamental STOV pulse of $l = 1$ is generated. Afterwards, thin beta barium borate (BBO) crystal plates are placed in both arms of a Mach–Zehnder setup. The reference pulse is

frequency-doubled Gaussian pulse. The STOV pulse after nonlinear conversion, is experimentally verified to be frequency-doubled with twice the transverse OAM per photon. The law of OAM conservation is valid if no SAM coupling is involved. The thickness of the BBO crystal affects the distortion caused by spatiotemporal astigmatism. Upconverted STOV pulse of $l=2$ displays a single hole and a 4π spiral phase for a thin (20 μm) BBO crystal, and two holes of 2π spiral phase for a thick (1 mm) BBO crystal. The SHG experiment with STOV pulses spurs interest of the investigation of nonlinear process with STOVs, such as stimulated Raman scattering, harmonic spin–orbit angular momentum conversion, and photonic entanglement generated by parametric process.

3.4 High harmonic generation (HHG)

High harmonic generation (HHG) is an extreme nonlinear process in light-matter interaction. HHG with transverse OAM driven by STOV pulses shows distinct features [63]. As shown in Fig. 1e, the spatial chirp of the fundamental STOV results in a significant tilt in HHG spectrum. The spatiotemporal singularity in STOV has an impact on electron subcycle dynamics leading to fringe patterns in the spectrum. The conservation of transverse OAM holds true for HHG if no spin–orbit coupling is involved. The spectral feature can be effectively controlled by two-color counterspin. The microscopic and macroscopic characteristics of HHG driven by transverse OAM provide a promising tool for attosecond science and extreme optics.

3.5 Dipole radiation theory

An infinitesimal dipole can be considered as an ideal point light source. Dipole models have been utilized in unidirectional excitation of electromagnetic guided modes and spin–orbit interaction via chiroptical responses [21, 64]. Focusing the complex conjugate of the radiation field emitted from an infinitesimal dipole results in a diffraction-limited spot. An array of infinitesimal dipoles with controllable relative amplitude, phase and oscillation direction digitize an optical focal field pixel by pixel (Fig. 1f). Both transversely oriented radially polarized and azimuthally polarized optical fields are demonstrated based on the time-reversal method and the vectorial diffraction theory. The 4Pi optical configuration is utilized to collect dipole radiation in all directions [65]. The superposition of transversely oriented radially polarized and azimuthally polarized leads to a controllable optical field carrying controllable transverse SAM and transverse OAM. It is worthy of noting that the generated field is not a propagating wave packet, but is stationary in the focal region.

4 Characterization of STOVs

Characterization of spatiotemporal optical fields is crucial for implementing structured ultrafast pulse as a key tool for microscopy, ultrafast manipulation, and attosecond science. Spatiotemporal metrology requires accurate 3D measurement of the amplitude, phase and polarization that change rapidly both in space and time. Spatiotemporal metrology measures both spatial and spectral information, and can be categorized into two methodologies: (1) spectrally resolved spectral/temporal measurement; (2) spatially-resolved spectral measurement techniques [66]. Scanning spectral/temporal measurement over space usually is unable to provide a full spatiotemporal measurement because these techniques are blind to the carrier-envelope relative phase and the pulse arrival time across space. A compact twofold spectral interferometer, based on in-line bulk interferometry and fiber-optic coupler assisted interferometry, is reported to measure infrared femtosecond vector beams with polarization evolving at the micrometer and femtosecond scales [67]. Digital holography has been demonstrated for spatiotemporal metrology in the terahertz spectrum [68, 69]. Techniques such as the total E-field reconstruction using a Michelson interferometer temporal scan (TERMITES) and INSIGHT are promising to become available products [70–72]. Considering the vector nature of electric fields, spatiotemporal vector beams provide additional challenge for characterization especially when the longitudinal electric components are prominent. The characterization of STOVs, however, is a less challenging task because only 2D information is required to measure and the wave packet is considered scalar with the electric field oscillating along the direction of the spatiotemporal phase singularity line. Differentiating STOVs of different topological charge usually does not require spatiotemporal metrology, and can be accomplished based on their diffraction properties [55].

4.1 Self-referenced interferometry technique

One easy-to-implement method is the self-referenced interferometry technique [29]. As shown in Fig. 2a, a STOV pulse is generated from a chirped wave packet. A reference pulse is split from the light source and dechirped through a grating pair. The reference pulse is transform-limited and considerably shorter than the STOV wave packet. The reference pulse is interfered with each temporal slice of the STOV wave packet using a motorized precision stage. Each interference pattern contains the information of a temporal slice of the STOV. The two-dimensional amplitude and phase information can be extracted through a Fourier filtering algorithm. The three-dimensional field information is reconstructed based on hundreds of two-dimensional temporal slices.

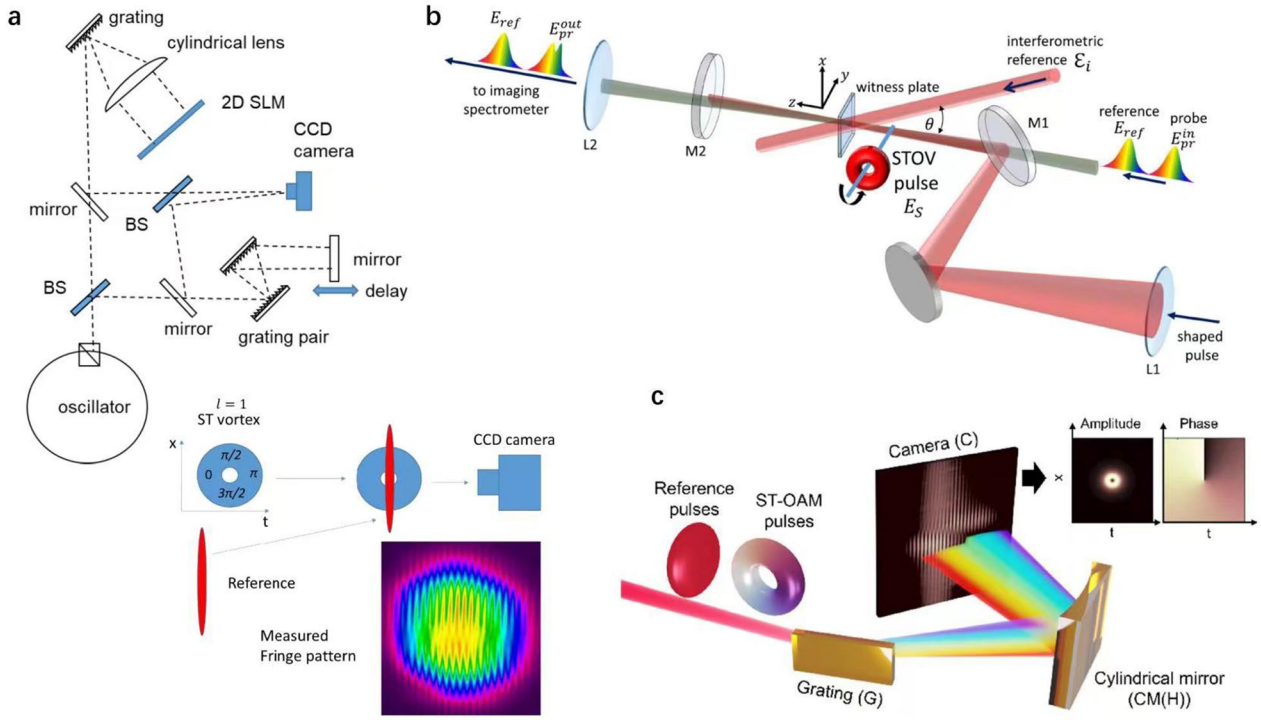

Fig. 2 Characterization of STOV wave packets. **a** Self-referenced interferometry technique. Adapted with permission from [29], copyright 2020, NPG. **b** Single-shot supercontinuum spectral interferometry. Adapted with permission from [28], copyright 2019, OPG. **c** Spatially resolved spectral interferometry. Adapted with permission from [73], copyright 2022, ACS

The interference patterns are vertical fringes at the beginning. As the slicing process moves toward the center of STOV, the vertical fringes begin to bend in the middle. As the reference pulse coincides with the spatiotemporal phase singularity of the STOV, the fringe pattern becomes two rows of fringes with a half-period shift that indicates a π phase difference between the upper and lower halves of the STOV. As the slicing process continues, the fringes start to bend in the other direction. The sequence of fringe bending directions is directly related to the sign of the topological charge of the STOV.

4.2 Single-shot supercontinuum spectral interferometry

STOVs are reported to be measured using single-shot supercontinuum spectral interferometry (Fig. 2b). Three beams are involved in the measurement: a STOV pulse, a supercontinuum probe pulse and a supercontinuum reference pulse. The STOV pulse causes phase modulation to the spatially and temporally overlapped chirped supercontinuum probe pulse in a thin fused silica plate (witness plate). The spatiotemporal phase imposed on the supercontinuum probe pulse is extracted in an imaging spectrometer using a supercontinuum reference pulse.

4.3 Spatially resolved spectral interferometry

Single-frame characterization of STOV pulses is accomplished using spatially resolved spectral interferometry [73]. The main characteristics such as the topological charge and helicity can be identified from the raw data. Other information including the pulse dispersion and beam divergence can be recovered after data processing and reconstruction. This characterization method enables single-shot measurements of ultrafast STOV pulses without requiring high pulse intensity.

5 Various types of spatiotemporal vortices

STOV wave packets exist in various forms that have additional spatiotemporal characteristics. The associated OAM density can be time-varying, oriented in arbitrary three dimensions. The STOV wave packets can be engineered to be propagation-invariant, or be shaped into a toroidal vortex form.

5.1 Time-varying STOV

Recently, Rego et al. demonstrated self-torqued beams carrying time-varying longitudinal OAM in extreme-ultraviolet spectrum [74]. Realizing wave packets carrying time-varying transverse OAM is also possible and in fact more straightforward [75]. Creating multiple

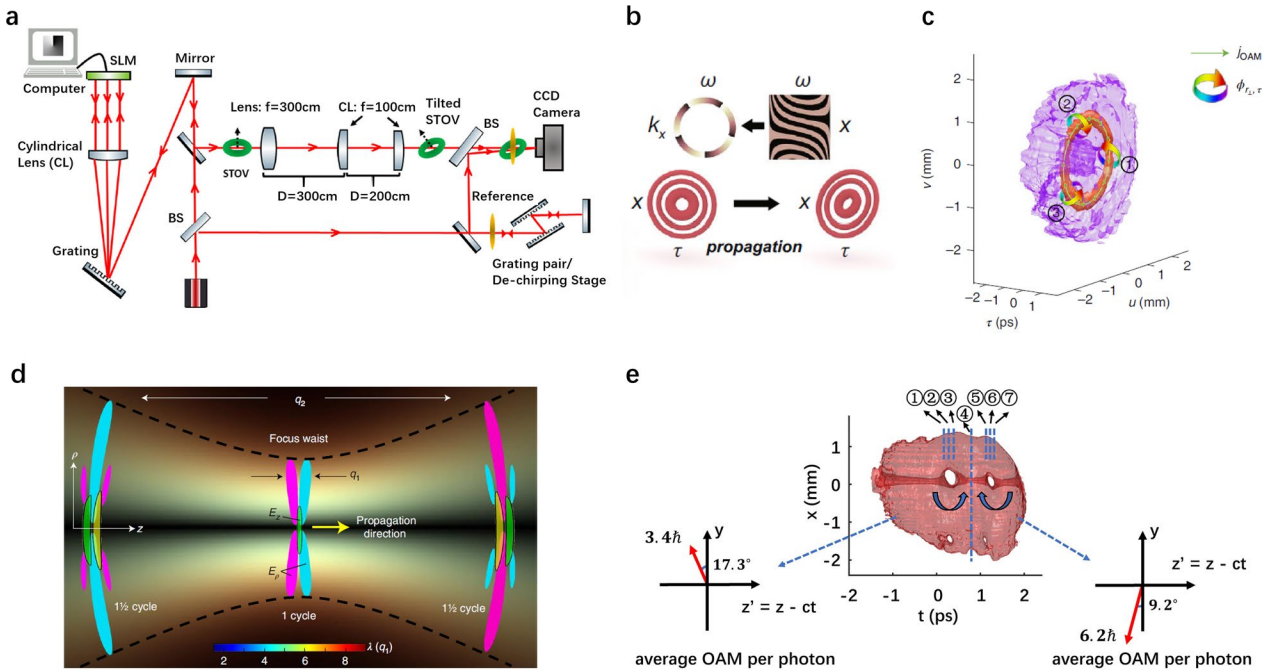

Fig. 3 Variants of STOV wave packets. **a** Creation of tilted STOVs using cylindrical lens system. Adapted with permission from [77], copyright 2022, De Gruyter. **b** Creation of degradation-free STOVs with high topological charge. Adapted with permission from [84], copyright 2022, NPG. **c** Conformal mapping reshapes a STOV tube to a toroidal vortex. Adapted with permission from [85], copyright 2022, NPG. **d** Toroidal vortex weaved by field lines and created by metasurfaces. Adapted with permission from [87], copyright 2022, NPG. **e** Intersection of spatial vortices and STOVs creates time-varying and 3D oriented average OAM. Adapted with permission from [89], copyright 2022, Oxford

spatially separated spatial vortices in the spatiotemporal frequency domain lead to multiple temporally separated STOVs within one wave packet. Each STOV can have different signs and values of topological charge. The OAM of the wave packet varies rapidly from head to tail. Experimental demonstration shows rapid transverse OAM alternation in the range from 0.5 to 1 ps.

5.2 Tilted STOV

Each photon within a STOV wave packet carries orbital angular momentum. The direction of the OAM is parallel to the phase singularity line and perpendicular to the light propagation direction. Since the discovery of transverse OAM, it is intriguing to explore plausible schemes to realize tilted STOVs with a tilted phase singularity line and OAM in arbitrary 3D directions.

The concept of a tilted STOV was first predicted using the special theory of relativity. A monochromatic spatial vortex beam emitted from a fast-moving source is seen by an observer as a tilted STOV [26]. This concept is interesting but difficult to experimentally realize it. Since the experimental realization of STOVs with transverse OAM, various schemes have been proposed and demonstrated to generate tilted STOVs. Photonic crystals with custom nodal lines are theoretically proposed to be capable of creating tilted STOVs [37].

Cylindrical lens system is commonly used as an astigmatic mode converter for transformation between Hermite Gaussian and Laguerre Gaussian modes [76]. Cylindrical lens system has been proven capable of coupling longitudinal OAM component to a STOV wave packet carrying pure transverse OAM to obtain a tilted STOV with a tilted OAM [77]. Figure 3a shows the experimental setup that utilizes cylindrical lens mode converter to create tilted STOVs. The tilt angle of the STOV is directed related to the rotation angle of the cylindrical lens pair. The tilt angle is limited to around 40° as the rotation angle of the mode converter increases to 80°. Further increase in the rotation angle causes the wave packet to break apart due to the asigmatic focusing effect.

Tilted STOVs carrying 3D oriented OAM have potential applications in high-speed optical communication [3, 78], generation of entangled tilted OAM states [79, 80], and light-matter interaction such as sculpting photocurrent distribution in semiconductors [81, 82].

5.3 Bessel-type STOV

STOV wave packets are 2D solutions to the Maxwell's equations that have spatiotemporal spiral phase. The

expression is a function of 1D spatial coordinate and 1D temporal coordinate. These solutions are analogues of well-studied spatial modes that are dependent on two spatial coordinates. A Bessel beam is a propagation-invariant with self-healing ability. A Bessel beam corresponds to a ring shape in the spatial frequency domain. An axicon can apply a conical phase to a plane wave and turns it into a Bessel beam. Similarly, a spatiotemporal Bessel wave packet can be generated by applying a spatio-spectral conical phase [83]. A Bessel STOV is a spatiotemporal Bessel wave packet that has a spatiotemporal spiral phase and multiple-ring structure for the intensity distribution in the spatiotemporal domain. If the dispersion and diffraction effects can be balanced using materials of custom dispersion parameters or using nonlinear process, the Bessel STOV is expected to have the central lobe propagation invariant both spatially and temporally for a long distance.

5.4 Degradation-free STOV

Higher-order STOVs are unstable and tend to split into a number of elemental STOVs upon free space propagation [54]. This phenomenon is attributed to spatiotemporal astigmatism, i.e. the wave packet broadens in the spatial dimension due to diffraction and undergoes no dispersion in the temporal dimension. The free space propagation is necessary for spatiotemporal Fourier transform and the degradation of high-order STOVs seems unavoidable. One solution to the problem is to view the SLM plane in a 2D pulse shaper (Fig. 1a) as the x–ω plane instead of k_x–ω plane and generate STOVs without free space propagation [84]. The generated STOVs corresponds to a circle on the light cone in contrast to a patch that is associated with a conventional STOV (Fig. 3b). The topological charge of the degradation-free STOVs is experimentally achieved up to 100.

5.5 Toroidal vortex

STOVs are spatiotemporal wave packets with 2D degrees of freedom: one spatial coordinate and one temporal coordinate. Transformation optics can be utilized to take a leap forward to the customization of 3D spatiotemporal wave packets. One interesting example is the demonstration of optical toroidal vortex [85, 86]. A toroidal vortex of light is a ring-shaped wave packet with poloidal spatiotemporal spiral phase. A STOV wave packet is elongated to a STOV tube and then conformally mapped to a toroidal vortex using transformation optics that completes log-polar to Cartesian mapping. The toroidal vortex is an approximate solution to the Maxwell's equations. The hollow core of the toroidal vortex corresponds to a circular phase singularity line (Fig. 3c).

A distinct type of toroidal vortex has a circular polarization singularity line [87]. The vectorial vortex ring has circulating electric (or magnetic) field lines surrounding the polarization singularity circle. Metasurfaces are fabricated to generate vectorial vortex rings in the terahertz domain. The longitudinal size of these vortex rings is wavelength-long, considerably shorter the transverse dimensions (Fig. 3d).

Numerical simulation has shown that tight focusing of cylindrical vector 2D-STOV wave packets lead to peculiar Yo–Yo ball like spatiotemporal distributions. Particularly, highly focused radially polarized 2D-STOV wave packet creates a transverse magnetic toroidal topology whereas highly focused azimuthally polarized 2D-STOV wave packet leads to transverse electric toroidal topology [88].

Although toroidal vortices of light are new, their analogues in fluid dynamics have been studied for a long time, such as the bubble rings, microbursts, and dandelion flying. Comparison of different types of toroidal vortices may bring insights to the study of photonic toroidal vortex in different aspects such as high-dimensional information carrier, toroidal mode excitation, and stable and high-energy pulses.

5.6 Collision of STOV and spatial vortex

A STOV wave packet can also embed an additional spatial vortex [89]. The phase singular lines of spatiotemporal and spatial vortices are crossed and normal to each other as shown by the iso-intensity plot (Fig. 3e). At the intersection, the two vortex tunnels intertwine with each other and both of them are bent with a bending direction dependent on the sign of the topological charge. The complex three-dimensional phase structure results in space-dependent angular momentum density. The average OAM per photon within the wave packet is determined by the topological charge of the spatiotemporal and spatial vortices as well as the intensity distribution of the wave packet. Both the value and the 3D orientation of average OAM per photon are fully controlled.

5.7 Partially coherent STOV

STOVs can be generated from a light source with partial temporal coherence with fluctuating temporal structures. Without the need of mode-locked laser sources, the partially coherent STOVs provide a cost-effective light source carrying transverse OAM.

Partially coherent vortex beams carrying longitudinal OAM have received much attention and found their applications in beam shaping, beam rotation and self-reconstruction. The description and propagation of STOVs with partial temporal coherence has been proposed by Hyde [90]. The experimental realization has also been accomplished recently [91]. The amplified spontaneous emission (ASE) is used as a partially coherent source and modelled

by applying a randomly distributed spectral phase and a Gaussian spectrum profile. As the phase randomness increases, the shape of the STOVs deviate from the ring-shaped profile with singularities occurring at various temporal locations. Amplitude fluctuations randomly spread throughout the whole temporal domain with multiple amplitude peaks. It is found that higher-order partially coherent STOVs break up into unitary vortices even without propagation. The instability of higher order partially coherent STOVs is an analog to the spatial vortex splitting caused by atmospheric turbulence [92]. An ytterbium-doped single-mode fiber laser with a central wavelength of 1030 nm is driven below the lasing threshold and the ASE is used as the light source for the experiment. The ASE from the single-mode fiber has a high degree of spatial coherence because only the fundamental transverse mode is lasing. The ASE state is temporally incoherent. Besides the ASE, a noise-like pulse (NLP) state from the fiber laser has also been investigated. The NLP state provides partial temporal coherence where the longitudinal modes are not strictly phase locked. The NLP state is generated through adjusting the nonlinear polarization evolution based saturable absorber. The spectrum width of the NLP state is 52 nm. STOVs generated from NLP states are useful for high-power applications because NLP states usually have higher peak power than ASE.

Both the spatial and temporal coherence of STOVs are reported to be controllable. It is found that the spatial and temporal coherence parameters play a vital role in controlling the phase distribution and position of a partially coherent STOV [93].

6 Applications of STOVs

STOV wave packets have spatiotemporal vortex shape and carry transverse OAM. New effects and phenomena are expected when this new degree of freedom for photons interacts with matter. Thus, quickly after its laboratory realization, the applications of STOVs in both fundamental physics and photonic engineering are being actively investigated.

6.1 Optical manipulation

Since the discovery of the connection of spatial spiral phase with longitudinal OAM, vortex beams have been vastly utilized in optical manipulation. The interaction between small particles and light carrying OAM generates light-induced toque and leads to rotation of particles. The conservation of angular momentum is a fundamental law that governs light-matter interaction. The transfer of angular momentum is generally limited to the direction parallel to the beam propagation direction. Nanoparticles can be rotated about the singularity line of a spatial vortex beam. Recently, the observation and measurement of transferring transverse spin and orbital angular momentum to micro particles of several micrometers in size are reported [94] (Fig. 4a). Transverse angular momentum transfer is especially advantageous in creating shear stress for studying mechanotransduction within the cell. STOVs carrying transverse OAM are expected to rotate particles about an axis that is perpendicular to the propagation direction of the wave packet and provide a versatile light source for transferring transverse OAM to small particles.

6.2 Interaction of transverse OAM with SAM

STOVs carry pure transverse intrinsic OAM. A Bessel-type STOV can be constructed using a superposition of plane waves with wave vectors distributed over a circle within the k_x–k_z plane [32]. These wave vectors have a spiral phase difference proportional to the topological charge l. The spectrum curve on the light cone of nondiffracting Bessel-type STOVs is an ellipse with the major axis parallel to k_z. The ellipse is Lorentz transform related to a circle. The electric field of each plane wave constituting Bessel-type STOVs must be orthogonal to its individual wave vector k. Two polarization situations, i.e. out of plane and in plane cases exist for Bessel-type STOVs. The out-of-plane polarization case is equivalent to the scalar case. The in-plane polarization case is less trivial because the electric field has both x and z components and is dependent on the wave vector of each plane wave (Fig. 4b). The interference of plane waves with different phase, spatial frequency and linear polarizations result in nonzero spin density indicating the presence of transverse spin. Despite the local spin–orbit interaction, the integral SAM vanishes and the integral OAM equals to $l\hbar$ per photon as long as the intensity distribution is circularly symmetric. If the intensity profiles deviate from circular symmetry, the OAM per photon is larger than $l\hbar$.

Tight focusing structured light and structuring STOVs in the focal region also involves the coupling of transverse OAM and SAM [34]. Using the Debye integral, the focal spot is calculated to have an intensity distribution in the shape of an elongated ring with a hollow core along the y-axis. The conversion from longitudinal SAM of the incident light to transverse OAM in the focused light occurs during the focusing process. The spin–orbit couplings involving transverse OAM are expected to be exploited in light-matter interactions.

6.3 Quantum optics

Semi-classical and approximate quantum theories break down when it comes to study structured single-photon pulses. The description of single photons with Stokes parameters and the Poincaré sphere ignores the vector

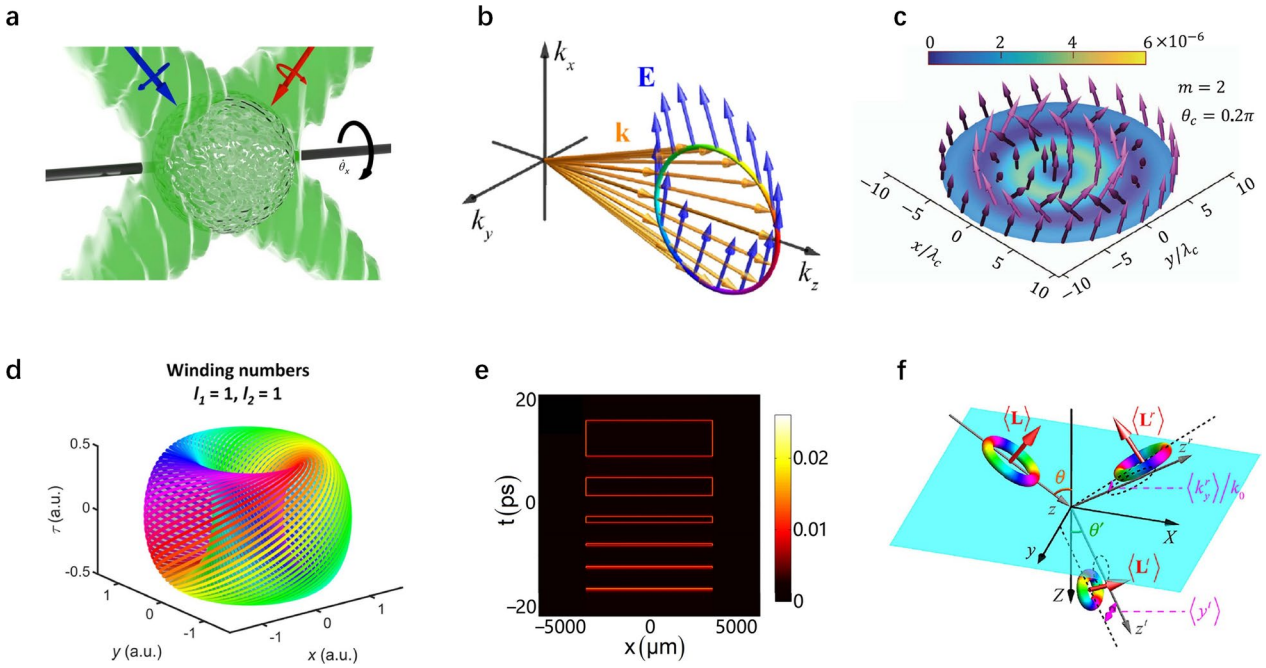

Fig. 4 Applications of STOV wave packets. **a** Rotation of birefringent microparticles with transverse OAM. Adapted with permission from [94], copyright 2022, NPG. **b** Local spin-orbit interaction for in-plane polarization Bessel-type STOVs. Adapted with permission from [32], copyright 2021, APS. **c** Helical spin-texture of a single-photon Bessel pulse. Adapted with permission from [95], copyright 2021, NPG. **d** Scalar optical hopfion weaved by equiphase lines. Adapted with permission from [96], copyright 2022, Springer. **e** Spatiotemporal differentiator with a spatial resolution of 18 μm and temporal resolution of 182 fs. Adapted with permission from [35], copyright 2022, WILEY. **f** Subluminal and superluminal pulse propagation of STOVs based upon Fresnel reflection/refraction. Adapted with permission from [97], copyright 2022, De Gruyter

nature of local spin and orbital AM densities. Recently, a framework is established based on quantum field theory to engineer the local angular momentum densities of quantum structured light pulse, especially for STOVs [95]. The quantum correlator of photonic spin density is introduced to characterize the nonlocal spin noise in light, facilitating the process of exploring exotic phases of light with long-range spin order. It is predicted that large fluctuations in the OAM along orthogonal directions exist in Bessel pulses with large OAM. This quantum noise is claimed to be veritable in metrology experiments with OAM laser beams. The quantum uncertainties $\hat{L}_x^{obs}$ and $\hat{L}_y^{obs}$ are linearly proportional to the photon number and proportional to the square of the helical phase index m in a Bessel pulse. The OAM fluctuations in the transverse plane are dependent on the polar angle of the Bessel pulse. It is demonstrated that the spin texture of a single-photon pulse can exhibit a very rich and interesting structure in the vectorial case (Fig. 4c). The spin density of a coherent pulse exhibit several features: the projection in the x–y plane is symmetric around the z-axis, leading the spatial integral to vanish; the projection in the x–y plane is either parallel or anti-parallel to the azimuthal unit vector, resulting in the helical spin texture; the projection in the x–y plane is described by the product of two Bessel functions and the clockwise and anti-clockwise structures oscillate in the spin texture; the sign of the z-component of spin is always positive (negative) for LCP (RCP) pulse, leading to the non-vanishing global spin.

6.4 Information carrier

Optical communication relies on the transmission of optical pulses to convey digital information. To expand the communication bandwidth, multiple physical quantities are incorporated, such as intensity, wavelength, phase and polarization. In the past couple of decades, increasing interest has been paid on the utilization of vortex beams carrying longitudinal OAM. The realization of transverse OAM undoubtedly adds an additional degree of freedom to OAM-based optical communication. More importantly, toroidal vortices are closely related to particle-like waves such as hopfions [96]. Hopfions are high dimensional particle-like waves that contain the information of stereographic projection from three-sphere (S^3) to two-sphere (S^2) (Fig. 4d). Using hopfions as information carrier will increase the information dimension per pulse for optical communication.

6.5 Spatiotemporal differentiator

As discussed in Sect. 3.2, 1D periodic structure that breaks the mirror symmetry has been designed to

generate STOVs [35]. Similar to topological spatial differentiator, this structure can be utilized as a spatiotemporal differentiator. The resolution of detecting sharp changes of 18 μm in the spatial coordinate and 182 fs in the temporal coordinate have been reported (Fig. 4e).

6.6 Slow light and fast light

Small shifts and time delays of wave packets such as Goos–Hänchen shift, Wigner time delay and spin-Hall effect have attracted increasing attention in nanophotonics. These shifts and time delays are typically on the scale of a wave period and can be extended to beam/pulse width through weak measurement technique. Vortex beams carrying longitudinal OAM have shown increased beam shifts by the factor of the topological charge. STOVs carry intrinsic transverse OAM exhibit peculiar properties of beam shifts and time delays depending on the value and orientation of the OAM [97]. Time delays become independent of the frequency enabling subluminal and superluminal pulse propagation without medium dispersion. The reflection/refraction of STOVs can be categorized into two cases: (A) the OAM is perpendicular to the incident plane; (B) the OAM lies within the incident plane (Fig. 4f). The normalized integral OAM of the incident pulse is given by,

$$\left\langle L^i \right\rangle = \frac{\gamma + \gamma^{-1}}{2} l, \tag{7}$$

where γ is the ellipticity of STOV and l is the topological charge. The STOV is inverted in the reflected pulse for case A and remains unchanged for case B. For the transmitted pulse, the STOV is stretched by a factor of $\frac{\cos\theta'}{\cos\theta}$ in the transverse direction and squeezed by a factor of $1/n$ in the longitudinal direction, where n is the relative refractive index. Paraxial polarized STOVs are assumed to experience all shifts known for Gaussian wave packets such as Goos–Hänchen and spin-Hall shifts. In addition, STOVs experience three additional shifts that are l-dependent. The first type is related to the conservation of the z-component of the total angular momentum. The orbital-Hall effect requires the transverse y-shift of the refracted pulse that generates an extrinsic OAM to compensate the imbalance between the z component of the intrinsic OAM between the incident and transmitted pulses. The typical scale of this shift is on the order of the wavelength and dependent on the topological charge l. The second type of shift is the angular Goos–Hänchen and spin-Hall shifts with an additional factor of $(1+|l|)$. The typical scale is independent of the ellipticity γ and is on the order of the inverse Rayleigh range. The third type of l-dependent shifts are the longitudinal shifts of STOVs reflected/refracted by a planar interface. These shifts are equivalent to time delays. However, unlike the Wigner time delays produced by temporal dispersion, these time delays originate from the spatial dispersion and thus are pure geometric phenomena. These time delays are be exploited to achieve subluminal and superluminal pulse propagation based upon Fresnel reflection/refraction instead of using dispersive media.

7 Summary and perspectives

Vortices are ubiquitous in nature. STOVs represent a novel type of optical vortices that have topological and conservative properties similar to spatial vortices as well as novel properties such as carrying transverse OAM. STOVs and their variants have exhibited peculiar photonic properties in various optical phenomena and become applicable in optical manipulation, spatiotemporal differentiator, subluminal and superluminal pulse propagation, and free space optical communication. Research remains to be done to fully understand the physical characteristics of these spatiotemporal phase singularities and explore their applications. Potential interesting topics include but certainly not limited to: propagation of STOVs via optical fibers and slab waveguides; reflection, refraction, and scattering of STOVs in nonuniform, anisotropic, or nonlinear materials; mode-excitation and light manipulation in nanostructures using STOVs; STOV-assisted dichroism for probing molecular chirality [98–100], optical parametric chirped-pulse amplification (OPCPA) of STOVs, characterization and applications of ultrafast and ultra-intense STOV pulses in light-matter interaction. It is always hard to predict the future of such a nascent research area that is rapidly developing. However, it is well expected that an increasing amount of physical mechanisms associated with STOVs are to be discovered and a wide range of applications are to be found in the near future.

Abbreviations

OAM	Orbital angular momentum
STOV	Spatiotemporal optical vortex
1D/2D/3D	One/two/three dimension
SAM	Spin angular momentum
SHG	Second harmonic generation
HHG	High harmonic generation
BBO	Beta barium borate
TERMITES	Total E-field reconstruction using a Michelson interferometer temporal scan
SLM	Spatial light modulator
OPCPA	Optical parametric chirped-pulse amplification
ASE	Amplified spontaneous emission
NLP	Noise-like pulse

Acknowledgements
Not applicable.

Author contributions
CW, AC and QZ wrote the manuscript. QZ supervised the project. All authors read and approved the final manuscript.

Funding
We acknowledge the support from the National Natural Science Foundation of China (NSFC) [92050202 (Q.Z.), 61875245 (C.W.)], Shanghai Science and Technology Committee [19060502500 (Q.Z.)], Wuhan Science and Technology Bureau [2020010601012169 (C.W.)], and the National Research Foundation of Korea (NRF) grant funded by the Korea government (MSIT) [2022R1A2C1091890 (A.C.)].

Data availability
All data presented in the report are available upon reasonable request.

Declarations

Ethics approval and consent to participate
Not applicable.

Consent for publication
Not applicable.

Competing interests
Authors declare no competing interests.

Received: 12 January 2023 Revised: 2 March 2023 Accepted: 5 March 2023
Published online: 29 May 2023

References

1. L. Allen, M.W. Beijersbergen, R.J.C. Spreeuw, J.P. Woerdman, Orbital angular momentum of light and the transformation of Laguerre–Gaussian laser modes. Phys. Rev. A **45**, 8185–8189 (1992)
2. A.M. Yao, M.J. Padgett, Orbital angular momentum: origins, behavior and applications. Adv. Opt. Photonics **3**, 161–204 (2011)
3. J. Wang et al., Terabit free-space data transmission employing orbital angular momentum multiplexing. Nat. Photonics **6**, 488–496 (2012)
4. M. Malik et al., Influence of atmospheric turbulence on optical communications using orbital angular momentum for encoding. Opt. Express **20**, 13195–13200 (2012)
5. A. Vaziri, G. Weihs, A. Zeilinger, Experimental two-photon, three-dimensional entanglement for quantum communication. Phys. Rev. Lett. **89**, 240401 (2002)
6. G. Molina-Terriza, A. Vaziri, J. Řeháček, Z. Hradil, A. Zeilinger, Triggered qutrits for quantum communication protocols. Phys. Rev. Lett. **92**, 167903 (2004)
7. M.E.J. Friese, J. Enger, H. Rubinsztein-Dunlop, N.R. Heckenberg, Optical angular-momentum transfer to trapped absorbing particles. Phys. Rev. A **54**(2), 1593 (1996)
8. M.E.J. Friese, H. Rubinsztein-Dunlop, J. Gold, P. Hagberg, D. Hanstorp, Optically driven micromachine elements. Appl. Phys. Lett. **78**, 547–549 (2001)
9. G. Nienhuis, Doppler effect induced by rotating lenses. Opt. Commun. **132**(1–2), 8–14 (1996)
10. B. Jack et al., Holographic ghost imaging and the violation of a bell inequality. Phys. Rev. Lett. **103**, 083602 (2009)
11. J.H. Lee, G. Foo, E.G. Johnson, G.A. Swartzlander, Experimental verification of an optical vortex coronagraph. Phys. Rev. Lett. **97**, 053901 (2006)
12. G.A. Swartzlander et al., Astronomical demonstration of an optical vortex coronagraph. Opt. Express **16**, 10200–10207 (2008)
13. K.Y. Bliokh, F. Nori, Transverse spin of a surface polariton. Phys. Rev. A **85**, 061801 (2012)
14. K.-Y. Kim, I.-M. Lee, J. Kim, J. Jung, B. Lee, Time reversal and the spin angular momentum of transverse-electric and transverse-magnetic surface modes. Phys. Rev. A **86**, 063805 (2012)
15. P. Banzer et al., The photonic wheel—demonstration of a state of light with purely transverse angular momentum. J. Eur. Opt. Soc. Rapid Publ. **8**, 13032 (2013)
16. K.Y. Bliokh, A.Y. Bekshaev, F. Nori, Extraordinary momentum and spin in evanescent waves. Nat. Commun. **5**, 3300 (2014)
17. J.P.B. Mueller, F. Capasso, Asymmetric surface plasmon polariton emission by a dipole emitter near a metal surface. Phys. Rev. B **88**, 121410 (2013)
18. C. Junge, D. O'Shea, J. Volz, A. Rauschenbeutel, Strong coupling between single atoms and nontransversal photons. Phys. Rev. Lett. **110**, 213604 (2013)
19. J. Petersen, J. Volz, A. Rauschenbeutel, Chiral nanophotonic waveguide interface based on spin–orbit interaction of light. Science **346**, 67–71 (2014)
20. D. O'Connor, P. Ginzburg, F.J. Rodríguez-Fortuño, G.A. Wurtz, A.V. Zayats, Spin–orbit coupling in surface plasmon scattering by nanostructures. Nat. Commun. **5**, 5327 (2014)
21. F.J. Rodríguez-Fortuño et al., Near-field interference for the unidirectional excitation of electromagnetic guided modes. Science **340**, 328–330 (2013)
22. F.J. Rodríguez-Fortuño et al., Universal method for the synthesis of arbitrary polarization states radiated by a nanoantenna: synthesizing arbitrary polarization states with a single nanoantenna. Laser Photonics Rev. **8**, L27–L31 (2014)
23. T. Bauer, S. Orlov, U. Peschel, P. Banzer, G. Leuchs, Nanointerferometric amplitude and phase reconstruction of tightly focused vector beams. Nat. Photonics **8**, 23–27 (2014)
24. M. Neugebauer, T. Bauer, A. Aiello, P. Banzer, Measuring the transverse spin density of light. Phys. Rev. Lett. **114**, 063901 (2015)
25. A.P. Sukhorukov, V.V. Yangirova, Spatio-temporal vortices: properties, generation and recording, in *Nonlinear Optics Applications*, vol. 5949, (SPIE, Bellingham, 2005), pp.35–43
26. K.Y. Bliokh, F. Nori, Spatiotemporal vortex beams and angular momentum. Phys. Rev. A **86**, 033824 (2012)
27. N. Jhajj et al., Spatiotemporal optical vortices. Phys. Rev. X **6**, 031037 (2016)
28. S.W. Hancock, S. Zahedpour, A. Goffin, H.M. Milchberg, Free-space propagation of spatiotemporal optical vortices. Optica **6**, 1547–1553 (2019)
29. A. Chong, C. Wan, J. Chen, Q. Zhan, Generation of spatiotemporal optical vortices with controllable transverse orbital angular momentum. Nat. Photonics **14**, 350–354 (2020)
30. S.W. Hancock, S. Zahedpour, H.M. Milchberg, Second-harmonic generation of spatiotemporal optical vortices and conservation of orbital angular momentum. Optica **8**, 594–597 (2021)
31. G. Gui, N.J. Brooks, H.C. Kapteyn, M.M. Murnane, C.-T. Liao, Second-harmonic generation and the conservation of spatiotemporal orbital angular momentum of light. Nat. Photonics **15**, 608–613 (2021)
32. K.Y. Bliokh, Spatiotemporal vortex pulses: angular momenta and spin–orbit interaction. Phys. Rev. Lett. **126**, 243601 (2021)
33. S.W. Hancock, S. Zahedpour, H.M. Milchberg, Mode structure and orbital angular momentum of spatiotemporal optical vortex pulses. Phys. Rev. Lett. **127**, 193901 (2021)
34. J. Chen, L. Yu, C. Wan, Q. Zhan, Spin–orbit coupling within tightly focused circularly polarized spatiotemporal vortex wavepacket. ACS Photonics **9**, 793–799 (2022)
35. J. Huang, J. Zhang, T. Zhu, Z. Ruan, Spatiotemporal differentiators generating optical vortices with transverse orbital angular momentum and detecting sharp change of pulse envelope. Laser Photonics Rev. **16**, 2100357 (2022)
36. C. Guo, M. Xiao, M. Orenstein, S. Fan, Structured 3D linear space–time light bullets by nonlocal nanophotonics. Light Sci. Appl. **10**, 160 (2021)
37. H. Wang, C. Guo, W. Jin, A.Y. Song, S. Fan, Engineering arbitrarily oriented spatiotemporal optical vortices using transmission nodal lines. Optica **8**, 966 (2021)
38. M. Yessenov, L.A. Hall, K.L. Schepler, A.F. Abouraddy, Space–time wave packets. Adv. Opt. Photonics **14**, 455–570 (2022)
39. K.Y. Bliokh et al., Roadmap on structured waves (2023), arXiv preprint arXiv:2301.05349
40. S. Akturk, X. Gu, P. Bowlan, R. Trebino, Spatio-temporal couplings in ultrashort laser pulses. J. Opt. **12**, 093001 (2010)
41. H.E. Kondakci, A.F. Abouraddy, Diffraction-free space–time light sheets. Nat. Photonics **11**, 733–740 (2017)
42. H.E. Kondakci, A.F. Abouraddy, Optical space–time wave packets having arbitrary group velocities in free space. Nat. Commun. **10**, 929 (2019)

43. M. Yessenov, L.A. Hall, S.A. Ponomarenko, A.F. Abouraddy, Veiled talbot effect. Phys. Rev. Lett. **125**, 243901 (2020)
44. M. Kulya, V. Semenova, A. Gorodetsky, V.G. Bespalov, N.V. Petrov, Spatio-temporal and spatiospectral metrology of terahertz broadband uniformly topologically charged vortex beams. Appl. Opt. **58**, A90–A100 (2019)
45. N.V. Petrov, B. Sokolenko, M.S. Kulya, A. Gorodetsky, A.V. Chernykh, Design of broadband terahertz vector and vortex beams: I. Review of materials and components. Light Adv. Manuf. **3**, 43 (2022)
46. N.V. Petrov, B. Sokolenko, M.S. Kulya, A. Gorodetsky, A.V. Chernykh, Design of broadband terahertz vector and vortex beams: II. Holographic assessment. Light Adv. Manuf. **3**, 44 (2022)
47. F. Eilenberger et al., Observation of discrete, vortex light bullets. Phys. Rev. X **3**, 041031 (2013)
48. Z. Bai, W. Li, G. Huang, Stable single light bullets and vortices and their active control in cold Rydberg gases. Optica **6**, 309–317 (2019)
49. T. Mayteevarunyoo, B.A. Malomed, D.V. Skryabin, Spatiotemporal dissipative solitons and vortices in a multi-transverse-mode fiber laser. Opt. Express **27**, 37364–37373 (2019)
50. G. Pariente, F. Quéré, Spatio-temporal light springs: extended encoding of orbital angular momentum in ultrashort pulses. Opt. Lett. **40**, 2037–2040 (2015)
51. M.V. Berry, Optical currents. J. Opt. Pure Appl. Opt. **11**, 094001 (2009)
52. K.Y. Bliokh, Orbital angular momentum of optical, acoustic, and quantum mechanical spatiotemporal vortex pulses. Phys. Rev. A **107**(3), L031501 (2023)
53. J. Chen, C. Wan, Q. Zhan, Engineering photonic angular momentum with structured light: a review. Adv. Photonics **3**, 064001–064001 (2021)
54. S. Huang, P. Wang, X. Shen, J. Liu, Properties of the generation and propagation of spatiotemporal optical vortices. Opt. Express **29**, 26995–27003 (2021)
55. S. Huang, P. Wang, X. Shen, J. Liu, R. Li, Diffraction properties of light with transverse orbital angular momentum. Optica **9**, 469–472 (2022)
56. Z. Jin et al., Phyllotaxis-inspired nanosieves with multiplexed orbital angular momentum. eLight **1**, 1–11 (2021)
57. J. Ni et al., Three-dimensional chiral microstructures fabricated by structured optical vortices in isotropic material. Light Sci. Appl. **6**, e17011 (2017)
58. Y. Bao, J. Ni, C. Qiu, A minimalist single-layer metasurface for arbitrary and full control of vector vortex beams. Adv. Mater. **32**, 1905659 (2020)
59. J. Ni et al., Multidimensional phase singularities in nanophotonics. Science **374**, eabj0039 (2021)
60. H. Namatsu, T. Yamaguchi, M. Nagase, K. Yamazaki, K. Kurihara, Nanopatterning of a hydrogen silsesquioxane resist with reduced linewidth fluctuations. Microelectron. Eng. **41**, 331–334 (1998)
61. D. Zhao, Z. Dong, K. Huang, High-efficiency holographic metacoder for optical masquerade. Opt. Lett. **46**, 1462–1465 (2021)
62. J. Huang, H. Zhang, T. Zhu, Z. Ruan, Topologically protected generation of spatiotemporal optical vortices with nonlocal spatial-mirror-symmetry-breaking metasurface (2022), Preprint at http://arxiv.org/abs/2206.01925
63. Y. Fang, S. Lu, Y. Liu, Controlling photon transverse orbital angular momentum in high harmonic generation. Phys. Rev. Lett. **127**, 273901 (2021)
64. J. Ni et al., Direct observation of spin–orbit interaction of light via chiroptical responses. Nano Lett. **22**, 9013–9019 (2022)
65. X. Meng, C. Wan, Q. Zhan, Transversely oriented cylindrically polarized optical fields. Opt. Express **30**, 14897–14909 (2022)
66. S.W. Jolly, O. Gobert, F. Quéré, Spatio-temporal characterization of ultrashort laser beams: a tutorial. J. Opt. **22**, 103501 (2020)
67. B. Alonso et al., Complete spatiotemporal and polarization characterization of ultrafast vector beams. Commun. Phys. **3**, 151 (2020)
68. J.T. Sheridan et al., Roadmap on holography. J. Opt. **22**, 123002 (2020)
69. Y.V. Grachev, V.A. Kokliushkin, N.V. Petrov, Open-source 3D-printed terahertz pulse time-domain holographic detection module. Appl. Opt. **61**, B307–B313 (2022)
70. C. Dorrer, Spatiotemporal metrology of broadband optical pulses. IEEE J. Sel. Top. Quantum Electron. **25**, 1–16 (2019)
71. G. Pariente, V. Gallet, A. Borot, O. Gobert, F. Quéré, Space–time characterization of ultra-intense femtosecond laser beams. Nat. Photonics **10**, 547–553 (2016)
72. A. Borot, F. Quéré, Spatio-spectral metrology at focus of ultrashort lasers: a phase-retrieval approach. Opt. Express **26**, 26444–26461 (2018)
73. G. Gui, N.J. Brooks, B. Wang, H.C. Kapteyn, M.M. Murnane, C.T. Liao, Single-frame characterization of ultrafast pulses with spatiotemporal orbital angular momentum. ACS Photonics **9**, 2802–2808 (2022)
74. L. Rego et al., Generation of extreme-ultraviolet beams with time-varying orbital angular momentum. Science **364**, eaaw9486 (2019)
75. C. Wan, J. Chen, A. Chong, Q. Zhan, Generation of ultrafast spatiotemporal wave packet embedded with time-varying orbital angular momentum. Sci. Bull. **65**, 1334–1336 (2020)
76. M.W. Beijersbergen, L. Allen, Astigmatic laser mode converters and transfer of orbital angular momentum. Opt. Commun. **96**, 123–132 (1993)
77. Y. Zang, A. Mirando, A. Chong, Spatiotemporal optical vortices with arbitrary orbital angular momentum orientation by astigmatic mode converters. Nanophotonics **11**, 745–752 (2022)
78. J. Wang, Advances in communications using optical vortices. Photonics Res. **4**, B14–B28 (2016)
79. A. Mair, A. Vaziri, G. Weihs, A. Zeilinger, Entanglement of the orbital angular momentum states of photons. Nature **412**, 313–316 (2001)
80. M. Erhard, R. Fickler, M. Krenn, A. Zeilinger, Twisted photons: new quantum perspectives in high dimensions. Light Sci. Appl. **7**, 17146 (2017)
81. S. Sederberg et al., Vectorized optoelectronic control and metrology in a semiconductor. Nat. Photonics **14**, 680–685 (2020)
82. A. Forbes, Sculpting electric currents with structured light. Nat. Photonics **14**, 656–657 (2020)
83. Q. Cao et al., Non-spreading Bessel spatiotemporal optical vortices. Sci. Bull. **67**, 133–140 (2022)
84. W. Chen et al., Time diffraction-free transverse orbital angular momentum beams. Nat. Commun. **13**, 4021 (2022)
85. C. Wan, Q. Cao, J. Chen, A. Chong, Q. Zhan, Toroidal vortices of light. Nat. Photonics **16**, 519–522 (2022)
86. F. Cardano, L. Marrucci, Smoke rings of light. Nat. Photonics **16**, 476–477 (2022)
87. A. Zdagkas et al., Observation of toroidal pulses of light. Nat. Photonics **16**, 523–528 (2022)
88. J. Chen, P. Zheng, Q. Zhan, Towards optical toroidal wavepackets through tight focusing of the cylindrical vector two dimensional spatiotemporal optical vortex. Opt. Express **30**, 46666–46679 (2022)
89. C. Wan, J. Chen, A. Chong, Q. Zhan, Photonic orbital angular momentum with controllable orientation. Natl. Sci. Rev. **9**, nwab149 (2022)
90. M.W. Hyde, Twisted space-frequency and space–time partially coherent beams. Sci. Rep. **10**, 12443 (2020)
91. A. Mirando, Y. Zang, Q. Zhan, A. Chong, Generation of spatiotemporal optical vortices with partial temporal coherence. Opt. Express **29**, 30426–30435 (2021)
92. M.P.J. Lavery, Vortex instability in turbulent free-space propagation. New J. Phys. **20**, 043023 (2018)
93. C. Ding et al., Source coherence-induced control of spatiotemporal coherency vortices. Opt. Express **30**, 19871–19888 (2022)
94. A.B. Stilgoe, T.A. Nieminen, H. Rubinsztein-Dunlop, Controlled transfer of transverse orbital angular momentum to optically trapped birefringent microparticles. Nat. Photonics **16**, 346–351 (2022)
95. L.-P. Yang, Z. Jacob, Non-classical photonic spin texture of quantum structured light. Commun. Phys. **4**, 221 (2021)
96. C. Wan, Y. Shen, A. Chong, Q. Zhan, Scalar optical hopfions. eLight **2**, 1–7 (2022)
97. M. Mazanov, D. Sugic, M.A. Alonso, F. Nori, K.Y. Bliokh, Transverse shifts and time delays of spatiotemporal vortex pulses reflected and refracted at a planar interface. Nanophotonics **11**, 737–744 (2022)
98. J. Ni et al., Gigantic vortical differential scattering as a monochromatic probe for multiscale chiral structures. Proc. Natl. Acad. Sci. **118**, e2020055118 (2021)
99. J.R. Rouxel et al., Hard X-ray helical dichroism of disordered molecular media. Nat. Photonics **16**, 570–574 (2022)
100. J. Ni et al., Giant helical dichroism of single chiral nanostructures with photonic orbital angular momentum. ACS Nano **15**, 2893–2900 (2021)